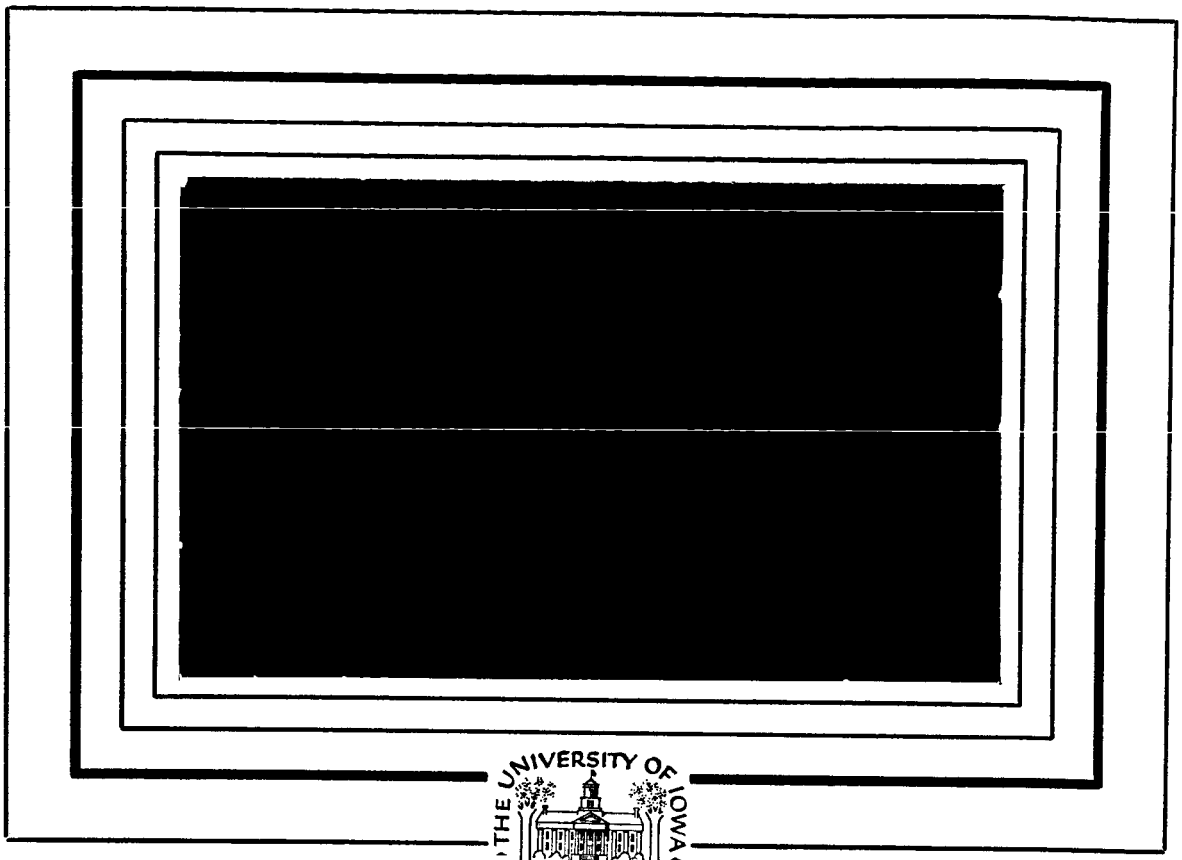

Department of Physics and Astronomy

THE UNIVERSITY OF IOWA

Iowa City, Iowa

U. of Iowa 66-9

Observations of Protons in the Magnetosphere with Mariner IV *

by

S. M. Krimigis and
T. P. Armstrong**

Department of Physics and Astronomy
University of Iowa
Iowa City, Iowa

March 1966

* This research has been supported in part by the National Aeronautics and Space Administration under Grant NsG-233-62.

** Graduate Trainee of National Aeronautics and Space Administration.

ABSTRACT 23516

On November 28, 1964, the Mariner IV spacecraft was launched towards Mars, and passed through the outer magnetosphere near the geomagnetic equatorial plane on the dawn side of the earth (sun-earth-probe angle about 112°). The University of Iowa experiment on Mariner IV consists in part of a thin (~ 35 microns) surface barrier detector with two discrimination levels; the detector is sensitive to protons in the energy ranges $0.50 \leq E_p \leq 11$ MeV (D_1) and $0.88 \leq E_p \leq 4$ MeV (D_2) and is quite insensitive to electrons of any energy (efficiency $\leq 10^{-7}$ for 40 keV electrons at counting rates of $\sim 10^6$ c/sec). The maximum proton intensities observed were $\sim 6 \times 10^7$ $(cm^2 \text{ sec sterad})^{-1}$ in D_1 for $2.97 \leq L \leq 3.80$ and 9.3×10^6 $(cm^2 \text{ sec sterad})^{-1}$ in D_2 for $L = 3.14$. Intensities significantly above background were detected for $1.88 \leq L \leq 13$ for D_1 and $1.88 \leq L \leq 7$ for D_2. The observed counting rates are consistent with a spectrum of the form $dj/dE = KE^{-\gamma}$ with γ increasing monotonically from 1.38 at $L \sim 2.35$ to ~ 8 at $L \sim 6.5$. The counting rates are also consistent with a spectrum of the form $dj/dE = Ke^{-E/E_o}$ with E_o decreasing monotonically from 740 keV at $L \sim 1.88$ to ~ 100 keV at $L \sim 6.5$. Observations of counting

rates vs L, and values of γ and E_o vs L are presented. These results represent a new body of measurements of trapped proton intensities near the equatorial plane in the magnetosphere at radial distances $\gtrsim 2.5\ R_e$ and have been obtained by a different detection scheme than that employed by Davis and Williamson [1963]. Our results are consistent with those of Davis and Williamson. The significance of the observations with respect to proposed theoretical models is discussed.

INTRODUCTION

Since the discovery of the Van Allen radiation belts, a large number of measurements have been made of the fluxes, energy spectrums, and the spatial distribution of charged particles throughout the magnetosphere. Specifically, outer zone protons of energy < 10 MeV have been studied by means of rockets [Bame et al., 1963] and satellites [Davis and Williamson, 1963; Fillius and McIlwain, 1964; Frank et al., 1964; Bostrom et al., 1965; Krimigis and Van Allen, 1965]. The present work is concerned with measurements of low energy ($\gtrsim$ 500 keV) protons obtained during the traversal of the earth's magnetosphere by the Mariner IV spacecraft.

The Mars-bound NASA-JPL Mariner IV spacecraft was launched successfully at 14:22 UT on November 28, 1964, and placed on a trajectory calculated to produce a close approach to the planet on July 15, 1965. The spacecraft trajectory through the magnetosphere is shown in Figure 1. The Sun-Earth-Probe (SEP) angle at which the spacecraft crossed the magnetospheric boundary (at 23 R_e) was 112.4 degrees, on the dawn side of the magnetosphere. After launch the orbit of the spacecraft rapidly approached the geomagnetic equatorial plane, and beyond ~ 3 R_e stayed continuously on this

plane. The University of Iowa proton detectors measured protons in two energy ranges, $0.50 \leq E_p \leq 11$ MeV and $0.88 \leq E_p \leq 4$ MeV. Proton measurements in these energy ranges have been reported before [Davis and Williamson, 1963] but did not extend to the magnetospheric boundary on the dawn side. In addition, the fact that the spacecraft stayed on the geomagnetic equator allowed the direct observation of the maximum directional intensities as a function of radial distance for protons in this energy range. The K_p daily sum for 28 November was 19_o and the K_p three hour index for the period when the detector counting rates were significantly above background was 3+.

Using the two data channels one can construct a two point energy spectrum which can be characterized by either a power law in energy with parameter γ, or an exponential in energy with parameter E_o; magnetic rigidity representations are also possible. Due to the fact that Mariner traversed the magnetosphere only once, one cannot separate the B and/or L dependence of the spectrum parameters except when certain assumptions are made; that is, the data are analyzed in the framework of some physical model. A comparison of the experimental data is made with the model of Nakada, Dungey, and Hess [1965] and the recent theoretical results of Nakada and Mead [1965]. Comparison is also made with the data of previous experimenters and a discussion of the significance of the results follows.

DETECTORS

The University of Iowa package of low energy particle detectors on Mariner IV consists of three end-window Geiger-Mueller tubes (EON Type 6213), designated A, B, and C (Table I); in addition, there is a surface barrier solid state detector (Nuclear Diodes, Inc.) designated D whose effective thickness is ~ 35 microns. The proton measurements reported in this paper were made exclusively with the solid state detector and a proper understanding of the data requires a description of the design and calibration of the instrument.

The design objectives for detector D were (a) to detect, pulse height analyze, and measure the absolute intensity of low energy (~ 500 keV) protons and (b) to make the detector insensitive to electrons of any energy. To satisfy these criteria a thin (35 micron) surface barrier solid state detector was chosen so as to minimize energy loss by penetrating electrons and the two energy discrimination levels were set far above the maximum energy loss for individual electrons. In addition, a fast-clipping pulse amplifier was used (Full Width at Half Maximum of 200 nanoseconds) to eliminate electron pile up. A block diagram of the electronics is shown in Figure 2. The voltage pulse presented at the output

of the charge sensitive pre-amplifier is clipped, amplified, and fed into the discriminators, which are set for the appropriate energy loss in the detector; pulses from the discriminators go into a rate limiter so that the counting rate will not exceed an upper limit, which in this case is chosen not to exceed the capacity of the spacecraft accumulators.

The detector used was of the surface barrier non-totally depleted type with a front window of negligible thickness ($\sim$ 40 micrograms/cm^2 of gold). The thickness of the detector is determined by the resistivity of the silicon used and the applied bias voltage. The properties of the detector were measured by use of alpha particles of well known energy and the bias voltage was set so that the thickness of the detector was 31 microns. The "effective" thickness, however, was about 35 microns, as can be seen from Figure 3; this is due to the fact that there is some collection of the charge which is produced beyond the depletion depth and which diffuses back into the space charge region [Mayer, 1961; Fillius; 1963]. This effect is quite noticeable for particles penetrating the sensitive region of the detector; it can be seen from Figure 3 that the energy loss is substantially higher than that expected for a 31 micron detector. Although we

do not have experimental points beyond ~ 3.6 MeV, we estimate that a penetrating proton of energy 10-11 MeV will leave enough energy (~ 420 keV) to be counted in the first discrimination level. The corresponding energy for the second discrimination level is 4 MeV.

To set the discrimination levels we have used the well established method of an alpha source and a pulser which is linear and stable to less than 0.1%. Once the levels were set the unit was placed in a proton beam and the efficiency vs energy profiles were directly established for each discrimination level. An example of the calibration is shown in Figure 4; here the ratio of input to output counting rate is plotted vs energy on probability paper because the efficiency can be approximated by an integral of the Gaussian

$$\epsilon\,(E) \;=\; \frac{1}{\sigma\sqrt{2\pi}} \int_{0}^{E} e^{-(E'-E_c)^2/2\sigma^2}\, dE' \qquad (1)$$

where E_c is the energy at the 50% point.

A plot of the efficiency on probability paper results in a straight line [Fillius, 1963]. It is seen that the mid-point (E_c) is at 495 keV, compared to 497 keV as determined by

the alpha source plus linear pulser method. The corresponding numbers for D_2 are 835 keV and 839 keV, respectively. The square root of the sum of the squares of the electronic noise and the detector resolution determine the FWHM which is typically 40 keV. It is seen that the discrimination levels when set by use of the alpha source and a linear pulser differ by less than 1% from those determined in a proton beam. The actual numbers for the unit that was flown on Mariner IV as determined by the linear pulser plus alpha source method are as follows:

D_1 - midpoint at 500 keV

D_2 - midpoint at 880 keV

FWHM = 43 keV

The thin detector, short clipping time, and high discrimination levels resulted in a negligible efficiency in counting electrons of any energy. A striking illustration of the electron insensitivity of the detector (in addition to pre-flight testing) is shown in Figure 5, where detector B (looking in the same direction as D_1) has been plotted on the same scale as D_1. It is seen that while B is saturated at 10 R_e (earth radii) due to the 40 keV electrons flux, D_1 is counting at about 3 times

background. The corresponding fluxes of particles seen by B and D_1 are about 2×10^7 $(cm^2 \text{ sec sterad})^{-1}$ and 2 $(cm^2 \text{ sec sterad})^{-1}$, respectively. The electron counting efficiency is therefore $< 10^{-7}$.

The physical configuration of the detector is as follows: it has a conical collimator with a full vertex angle of 60°. The sidewall shielding of the detector has a minimum thickness corresponding to the range of ~ 50 MeV protons. In order to shield against sunlight a nickel foil, whose thickness is 0.22 mg/cm^2 of air equivalent for alpha particles, was placed in front of the detector. The effect of the foil is properly taken into account when the discrimination levels are set. Knowledge of the proper operation of the instrument is assured through an inflight $_{95}Am^{241}$ source of 5.477 MeV alpha particles, which was goldplated in order to obtain a falling spectrum between 500 keV and 880 keV. Thus, any change in the detector characteristics and/or drift in the discrimination levels would have been immediately noticeable; a preliminary inspection of the data has shown no such change over the 10-month period of operation of the instrument. Because the thin detector collects only a few tens of keV from a minimum ionizing particle, the contribution of cosmic rays to the

background counting rate for particles coming in through the collimator is negligible. The contribution to the background counting rate for particles coming in through the shielding and crossing the detector sideways is about three orders of magnitude less than the background counting rate due to the inflight source.

RESULTS

(a) General Remarks

During the magnetospheric passage the -Z axis of the Mariner IV spacecraft was pointing continuously at the sun. The axis of detector D makes an angle at 70° to the spacecraft -Z axis, i.e., the angle between the detector axis and the spacecraft-sun line is 70°. The spacecraft was rotating about the Z axis with a period of approximately 30 minutes (L. Davis, Jr., private communication). Thus, the orientation of the detector axis with respect to the $\vec{B}$ vector was changing with time so that the detector was sampling particles of various pitch angles at different times. An accompanying experiment on the spacecraft was a triaxial helium magnetometer which provided information on the magnitude and direction of the magnetic field vector in spacecraft coordinates beyond a geocentric distance of $\sim 4.5\ R_e$ (Ed. Smith, private communication). At distances closer than $4.5\ R_e$ the modulation of telemetry signal strength was used (D. E. Jones, private communication) which, combined with the later magnetometer data, gives the orientation of the detector with respect to the $\vec{B}$ vector, with sufficient accuracy for the purpose of this experiment.

Figures 6 and 7 show our measured directional intensity of protons as a function of L in the indicated energy ranges, as well as the orientation of the detector with respect to the $\vec{B}$ vector, and the degree of departure of the trajectory from the geomagnetic equator in B/B_o, the two magnetic coordinates being those of McIlwain [1961]. The solid curve in the intensity vs L profile represent the actual intensities observed at various pitch angles; the dotted curve is the line drawn between points at which the detector axis was perpendicular to the $\vec{B}$ vector, and thus represents the interpolated intensity of particles whose velocity vector is perpendicular to the magnetic field. The intensity was significantly above background when the detector was turned on at L ~ 1.88 and rose very sharply (by 10^6 in $\Delta L \simeq 0.5$) until channel D_1 became saturated between L of 2.9 to 3.8. We have estimated the peak intensity of protons to be 6×10^7 $(cm^2 \text{ sec sterad})^{-1}$ to within $\pm$ 30% at L ~ 3.1 by using the non-saturated counting rate of channel D_2 and an interpolated value of E_o, the spectral parameter. Figure 6 extends to L = 13, beyond which the intensity of protons is not significantly above background as can be seen from Figure 5. The intensity vs L profile for protons in the range $0.88 \leq E_p \leq 4$ MeV is shown in

Figure 7 and has the same general characteristics as that for protons in the range of $0.50 \leq E_p \leq 11$ MeV, as described above. The intensity is significantly above background to $L \sim 7.1$.

It is noted from the B/B_o vs L graph that beyond $L \sim 3$ the trajectory of the spacecraft remained in the geomagnetic equatorial plane, so that the observed particle intensity perpendicular to $\vec{B}$ is the maximum intensity along a given L shell, as established by experimental observations of the equatorial pitch angle distributions.

(b) Angular Distribution

As can be seen from Table 1, the conical collimator of the detector has a half angle of 30°, so that the observed counting rate represents an integral of proton intensity over a 60° sector of the solid angle centered about the collimator axis. By correlating the modulation of counting rates in Figures 6 and 7 with the angle between collimator axis and the B-vector, it can been seen that the proton intensity is a function of pitch angle α. It is possible to derive a rough estimate of the form of $j_p(\alpha)$ at a given value of L by using the ratio of the observed $\overline{j_p(\alpha)}$

to the interpolated $\overline{j_p(90°)}$ where the bar represents an integral over the collimator angle. It is convenient to assume the form $\sin^n\alpha$ for the pitch angle distribution and to derive a value of n from the observed ratios. The $\sin^n\alpha$ form can be assumed to apply with a single value of n only over a limited pitch angle range [e.g., see Davis and Williamson, 1963]. Hence the present observation is seriously limited by the wide (60°) opening angle of the detector and for this reason a detailed calculation has proved inconclusive. The data, however, are consistent with $n = 3 \pm 1$, with the value of n subject to the limitations noted above.

(c) Energy Spectrum

Due to the fact that there exist observations at only two energies, it is not possible to uniquely determine the functional form of the energy spectrum. We have used the two commonly assumed forms, namely $dj/dE = Ke^{-E/E_o}$ and $dj/dE = KE^{-\gamma}$, and have computed values for E_o and γ, respectively. The results are shown as a function of L in Figure 8, where a plot of B/B_o is also included. Statistical uncertainty in the values of E_o and γ is shown whenever it exceeds the diameter of the point. The points shown during the

time when D_1 was saturated represent lower limits for γ and upper limits for E_o. The values of E_o range from about 740 keV at $L \sim 1.88$ to about 100 keV at $L \sim 6.5$. The values of γ range from 1.38 at $L \sim 2.35$ to about 8 at $L \sim 6.5$. For $L \leq 2.27$ it is not possible to fit the observed ratios to a power law spectrum. This implies that the spectrum may not be falling monotonically below $L \leq 2.27$. Although the last result is statistically significant, the inconsistency with a power law spectrum is not compelling if the uncertainty in the high energy cutoff of the detector is taken into account.

It can be seen from Figure 8 that the spectral parameters E_o and γ vary, as both B/B_o and L change along the spacecraft trajectory. It is thus not possible, in principle, to separate the B and/or L dependences. However, the scatter in the data produced by the sampling of different pitch angles as the spacecraft rotates is much smaller than the total apparent variation of the spectral parameter with L. Indeed the range of the observed equatorial pitch angles corresponded to a much larger equivalent variation of B/B_o than that actually encountered. It is thus possible to conclude that the variation of the spectral parameters with B is not important compared to their variation with L in this set of observations.

DISCUSSION

(a) Comparison with Other Measurements

The results of this experiment may be compared with proton measurements in the energy range $0.12 \leq E_p \leq 4.5$ MeV made by Davis and Williamson [1963]. An appropriate point for comparison was obtained in their pass closest to the geomagnetic equator (~ 7 degrees) at $L \sim 3.1$ where their reported intensity was $\sim 6 \times 10^7$ $(cm^2 \text{ sec sterad})^{-1}$ with an accuracy of $\pm 50\%$. Our corresponding number is also 6×10^7 $(cm^2 \text{ sec sterad})^{-1}$ at the geomagnetic equator. If we take into account the difference in the energy intervals observed and in the values of B/B_o, the two measurements seem to agree well.

(b) Energy Density

It is of interest to consider the energy density of the observed protons and the relation between particle and field energy densities. The present set of measurements is complementary to those used by Hoffman and Bracken [1965] in computing the magnetic effects of the quiet-time proton belt. One may compute the particle energy density W_p by using the observed angular distribution and taking into account the particle energy spectrum. One has

$$W_p = 2\pi \int_{-\frac{\pi}{2}}^{+\frac{\pi}{2}} \int_{0.5}^{11\ \mathrm{MeV}} \frac{E}{\sqrt{2E/m}} \left(\frac{dj}{dE}\right) dE\ \sin^{n+1}\alpha\ d\alpha$$

It is explicitly assumed here that the energy spectrum is independent of pitch angle. At $L \sim 3.1$, the e-folding energy $E_o \simeq 200$ keV and the power law parameter $\gamma \simeq 5$. Substituting for dj/dE an exponential form and a power law, respectively, as determined earlier, we find that

$W_p \simeq 4 \times 10^{-7}$ ergs/cm^3 (exponential in energy)

$0.5 \leq E_p \leq 11$ MeV

$W_p \simeq 8 \times 10^{-7}$ ergs/cm^3 (power law in energy)

In the above calculation the value $n = 3$ was used for the angular distribution of intensity as discussed earlier in this paper.

The magnetic field energy density W_F on the equator at $L \sim 3.1$ is given by

$$W_F = \frac{B^2}{8\pi} = 6.65 \times 10^{-6}\ \mathrm{ergs/cm^3}\ .$$

The ratio of particle to magnetic field energy density at the equator is then

$R = \frac{W_P}{W_F} = 0.06$ (exponential in energy)

$0.5 \leq E_p \leq 11$ MeV

$R = \frac{W_P}{W_F} = 0.12$ (power law in energy)

It is seen that particle energy density can be as large as 5 to 10% of the field energy density. It should be noted that the numbers quoted above should be considered as a lower limit, since the detector threshold is at 500 keV and the e-folding energy of the spectrum at $L \sim 3.1$ is about 200 keV. A plot of the computed proton energy (using the assumption outlined above) is shown in Figure 9. It is obvious that the ratio of the 500 keV proton energy density to the field energy density is not a constant and decreases with increasing L, for $L > 3.1$. Some and perhaps all of the variation in the ratio as a function of L may be accounted for by protons which are below the energy threshold of the detector.

(c) Comparison with Theory

It has been shown in the past that the observed numbers of low energy protons cannot be explained in terms of either CRAND (Cosmic Ray Albedo Neutron Decay) or SPAND (Solar Proton Albedo Neutron Decay) [Bostrom et al., 1965; Fillius, 1965]. Recently, interest has turned to the solar wind as a possible source and the early ideas of Kellogg [1959], Parker [1960], and Herlofson [1960] have been further examined by Davis and Chang [1962],

Tverskoy [1964], Nakada et al. [1965], and Nakada and Mead [1965]. The mechanism is that of injection of particles, usually at the magnetospheric boundary, with subsequent inward diffusion and energization by conserving the first two adiabatic invariants and violating the third.

The calculations of Nakada et al. [1965] show that the energy spectrum parameter E_o should vary as L^{-3} at the equator for particles whose pitch angle is 90°. In Figure 10 the observed value of E_o has been plotted as a function of L in a logarithmic plot; a line with slope of -3 has been drawn for comparison. It is seen that there is fair agreement with the L^{-3} law for L in the range from 2 to 4, with the scatter in the points attributable to the variation of E_o with pitch angle. Beyond L of 4 there is an apparent discontinuity in the curve which may be connected with the observation that the spectrum is a double exponential described by two different values of E_o [Hoffman and Bracken, 1965].

Nakada and Mead [1965] have used a Fokker-Planck diffusion equation with terms describing Coulomb energy degradation and charge-exchange losses with the ambient atmosphere; in this manner, they are able to obtain radial and energy distributions for trapped

protons in the outer zone. Our results, obtained in the geomagnetic equator, can be compared directly to their calculated intensity vs. distance profiles (see their Figure 8, curve No. 5). It is observed that there is general qualitative agreement between the predicted and observed intensity-distance profiles. The peak calculated intensity, however, appears to be at a higher L value than the observations indicate. In addition, the decrease of intensity from maximum towards higher L values as predicted by the model is less than that shown by the observations. It would appear that the Coulomb loss rate is greater than that assumed in the calculation. As the authors remark, however, a re-evaluation of the parameters used in the computation can make important quantitative differences in the shape of the curves.

ACKNOWLEDGEMENTS

Development, construction, and pre-flight testing of the University of Iowa equipment was supported by subcontract 950613 with the Jet Propulsion Laboratory. Analysis and publication have been performed in part under National Aeronautics and Space Administration Grant NsG 233-62. We thank Dr. J. A. Van Allen for his continuous encouragement and useful comments throughout this work. We are indebted to Dr. L. A. Frank and Messrs. H. K. Hills, D. L. Chinburg, D. C. Enemark, and E. W. Strein of the University of Iowa, and to Dr. H. R. Anderson and Messrs. R. K. Sloan, R. A. Lockhart, and D. K. Schofield of the Jet Propulsion Laboratory for various aspects of the work. We also thank the Mariner IV magnetometer experimenters, Drs. E. Smith, L. Davis, D. Jones, and P. Coleman, for providing information on the orientation of the spacecraft with respect to the $\vec{B}$ vector.

REFERENCES

Bame, S. J., J. P. Conner, H. H. Hill, and F. E. Holly, Protons in the Outer Zone of the Radiation Belt, J. Geophys. Res., 68, 55-63, 1963.

Bostrom, C. O., A. J. Zmuda, and G. F. Pieper, Trapped Protons in the South Atlantic Magnetic Anomaly, July through December, 1961. 2. Comparisons with Nerv and Relay I, and the Energy Spectrum, J. Geophys. Res., 70, 2035-2044, 1965.

Davis, Leverett, and D. B. Chang, On the Effect of Geomagnetic Fluctuations on Trapped Particles, J. Geophys. Res., 67, 2169-2179, 1962.

Davis, L. R., and J. M. Williamson, Low-Energy Trapped Protons, Space Research III, Proceedings of the Third International Space Science Symposium, North-Holland Publishing Company, Amsterdam, 1963, pp. 365-375.

Fillius, R. W., Satellite Instruments using Solid State Detectors, Research Report SUI 63-26, Department of Physics and Astronomy, University of Iowa, Iowa City, Iowa, 1963.

Fillius, R. W., and C. E. McIlwain, Anomalous Energy Spectrum of Protons in the Earth's Radiation Belt, Phys. Rev. Letters, 12, 609-612, 1964.

Fillius, R. W., Trapped Protons of the Inner Radiation Belt, J. Geophys. Res., 71, 97-123, 1966.

Frank, L. A., J. A. Van Allen, and H. K. Hills, A Study of Charged Particles in the Earth's Outer Radiation Zone with Explorer 14, J. Geophys. Res., 69, 2171-2191, 1964.

Freden, S. C., J. B. Blake, and G. A. Paulikas, Spatial Variation of the Trapped Proton Spectrum, J. Geophys. Res., 70, 3113-3116, 1965.

Herlofson, N., Diffusion of Particles in the Earth's Radiation Belts, Phys. Rev. Letters, 5, 414-416, 1960.

Hoffman, R. A., and P. A. Bracken, Magnetic Effects of the Quiet-Time Proton Belt, J. Geophys. Res., 70, 3541-3556, 1965.

Kellogg, P. J., Van Allen Radiation of Solar Origin, Nature, 183, 1295, 1959.

Krimigis, S. M., and J. A. Van Allen, Observations of Geomagnetically Trapped Protons with Injun 4 (Abstract), Trans. Am. Geophys. Union, 46 (1), 140, 1965.

McIlwain, C. E., Coordinates for Mapping the Distribution of Magnetically Trapped Particles, J. Geophys. Res., 66, 3681-3691, 1961.

Mayer, J. W., Pulse Formation in Semi-conductor Detectors, Proceedings of the Ahserville Conference, 1961.

Nakada, M. P., J. W. Dungey, and W. N. Hess, On the Origin of Outer-Belt Protons, 1, J. Geophys. Res., 70, 3529-3532, 1965.

Nakada, M. P., and G. D. Mead, Diffusion of Protons in the Outer Radiation Belt, J. Geophys. Res., 70, 4777-4791, 1965.

Parker, E. N., Geomagnetic Fluctuations and the Form of the Outer Zone of the Van Allen Radiation Belt, J. Geophys. Res., 65, 3117-3130, 1960.

Tverskoy, V. A., Dynamics of the Radiation Belts of the Earth, 2, Geomagnetism and Aeronomy, 3, 351-366, 1964.

Table I

Characteristics of Detectors

Detector	Unidirectional Geometric Factor, cm^2 ster	Omnidirectional Geometric Factor, cm^2	Particles to Which Sensitive	Dynamic Range
A	0.044 ± 0.005	~ 0.15	Electrons: $E_e \gtrsim 45$ keV Protons: $E_p > 670 \pm 30$ keV	From galactic cosmic ray rate of 0.6 counts/sec to 10^7 counts/sec
B	0.055 ± 0.005	~ 0.15	Electrons: $E_e \gtrsim 40$ keV Protons: $E_p > 550 \pm 20$ keV	"
C	0.050 ± 0.005	~ 0.15	Electrons: $E_e \gtrsim 150$ keV Protons: $E_p > 3.1$ MeV	"
D_1	0.065 ± 0.003	---	Electrons: None Protons: $0.50 \leq E_p \leq 11$ MeV	From in-flight source rate to 10^6 counts/sec
D_2	0.065 ± 0.003	---	Electrons: None Protons: $0.88 \leq E_p \leq 4.0$ MeV	"

FIGURE CAPTIONS

Figure 1 - Mariner IV trajectory through the magnetosphere. The sun-earth-probe angle was 112.4 degrees as the spacecraft crossed the boundary at 23 R_e.

Figure 2 - Pulse height analysis scheme for the University of Iowa solid state detector on Mariner IV.

Figure 3 - Energy lost in detector vs incident kinetic energy for protons, for a standard Mariner IV solid state detector. Note the discrepancy between the calculated and experimental curve for penetrating particles.

Figure 4 - Typical energy passband of Mariner IV detector series. Plot on probability graph paper results in a straight line.

Figure 5 - An illustration of the insensitivity of the solid state detector to counting electrons. The efficiency is less than 1×10^{-7} at counting rates of 10^6 counts/second.

Figure 6 - Trapped proton intensity in the energy range $0.5 \leq E_p \leq 11$ MeV as a function of L. Notice that the spacecraft trajectory was close to the geomagnetic equator as evidenced from the B/B_o curve.

Figure 7 - Trapped protons in the energy range $0.88 \leq E_p \leq 4$ MeV as a function of L.

Figure 8 - The spectral parameters of the measured protons as a function of L.

Figure 9 - The energy density of protons in the range $0.500 \leq E_p \leq 11$ MeV as a function of L. A pitch angle distribution of $\sin^3 \alpha$ and a power law spectrum have been assumed in the computation.

Figure 10 - Comparison of the experimental results with the model of Nakada, Dungey, and Hess.

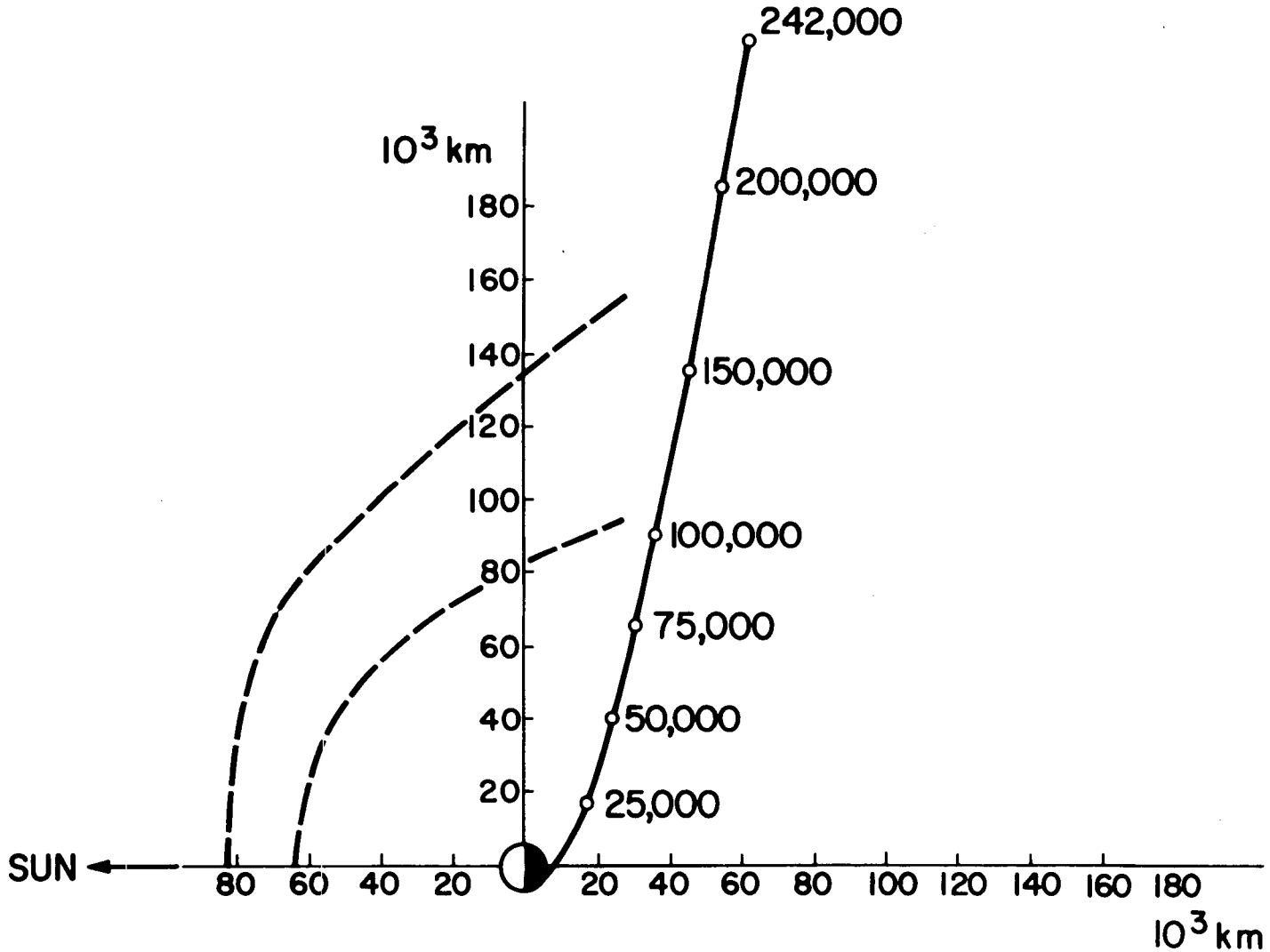

Figure 1

MARINER IV NEAR-EARTH TRAJECTORY

G 65-323

BLOCK DIAGRAM OF MARINER IV
SOLID STATE DETECTOR ELECTRONICS

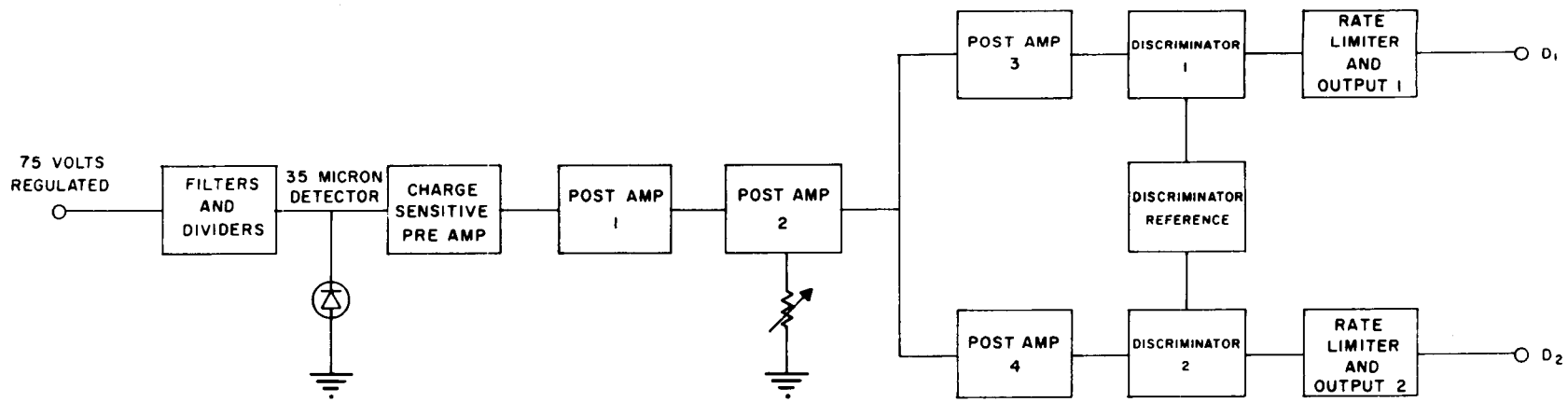

Figure 2

TYPICAL MARINER IV PULSE HEIGHT ANALYSIS SCHEME USING A 31 MICRON SURFACE BARRIER DETECTOR WITH NICKEL FOIL IN FRONT

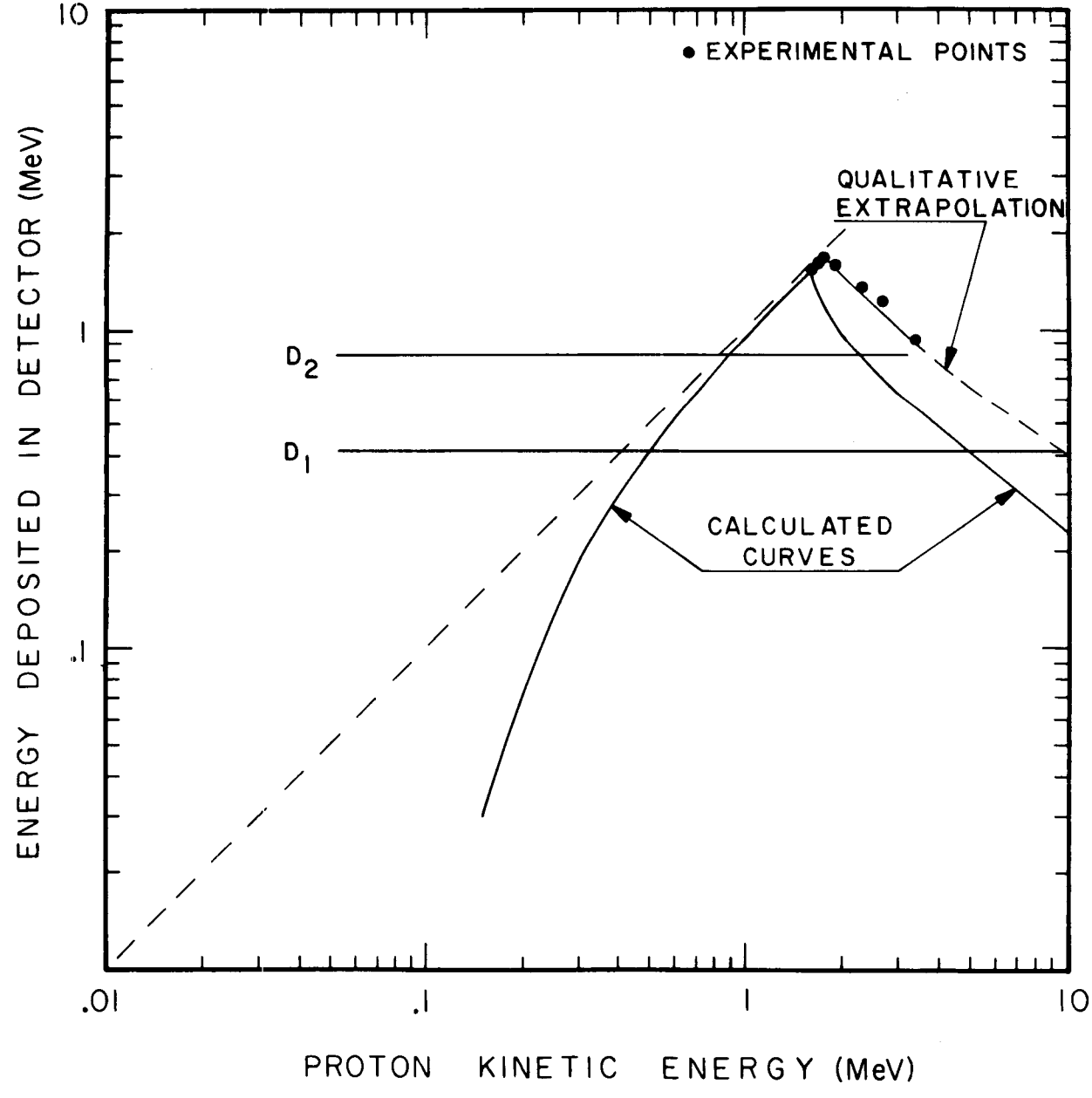

Figure 3

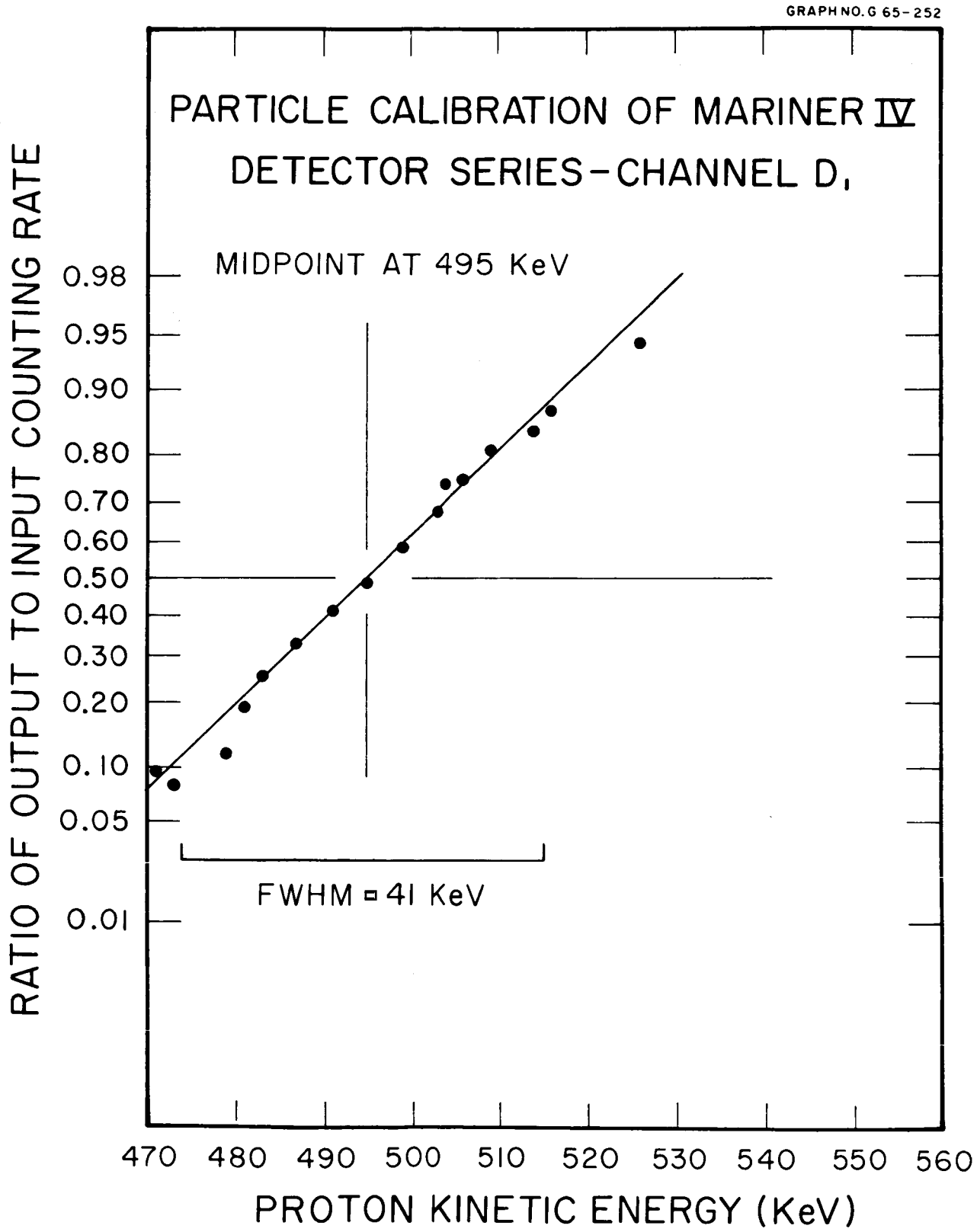
GRAPH NO. G 65-252
PARTICLE CALIBRATION OF MARINER IV
DETECTOR SERIES-CHANNEL D,
MIDPOINT AT 495 KeV
FWHM = 41 KeV
RATIO OF OUTPUT TO INPUT COUNTING RATE
0.98
0.95
0.90
0.80
0.70
0.60
0.50
0.40
0.30
0.20
0.10
0.05
0.01
470
480
490
500
510
520
530
540
550
560
PROTON KINETIC ENERGY (KeV)

Figure 4

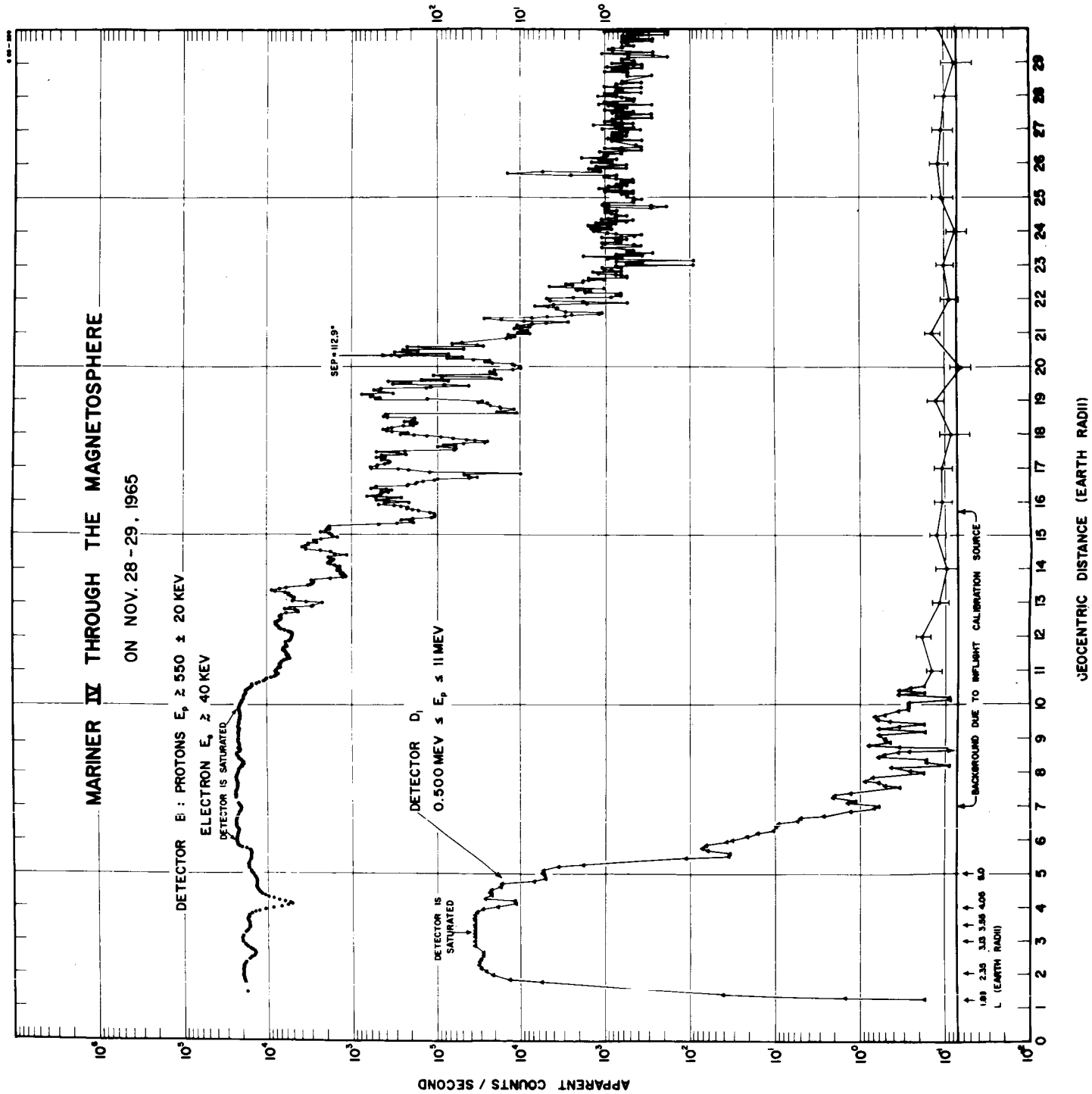
MARINER IV THROUGH THE MAGNETOSPHERE
ON NOV. 28-29, 1965
DETECTOR E1 : PROTONS Ep ≥ 550 ± 20 KEV
ELECTRON Ep ≥ 40 KEV
DETECTOR IS SATURATED
DETECTOR D1
0.500 MEV ≤ Ep ≤ 11 MEV
DETECTOR IS SATURATED
SEP = 112.9°
BACKGROUND DUE TO INFLIGHT CALIBRATION SOURCE
L (EARTH RADII)
APPARENT COUNTS / SECOND
GEOCENTRIC DISTANCE (EARTH RADII)

Figure 5

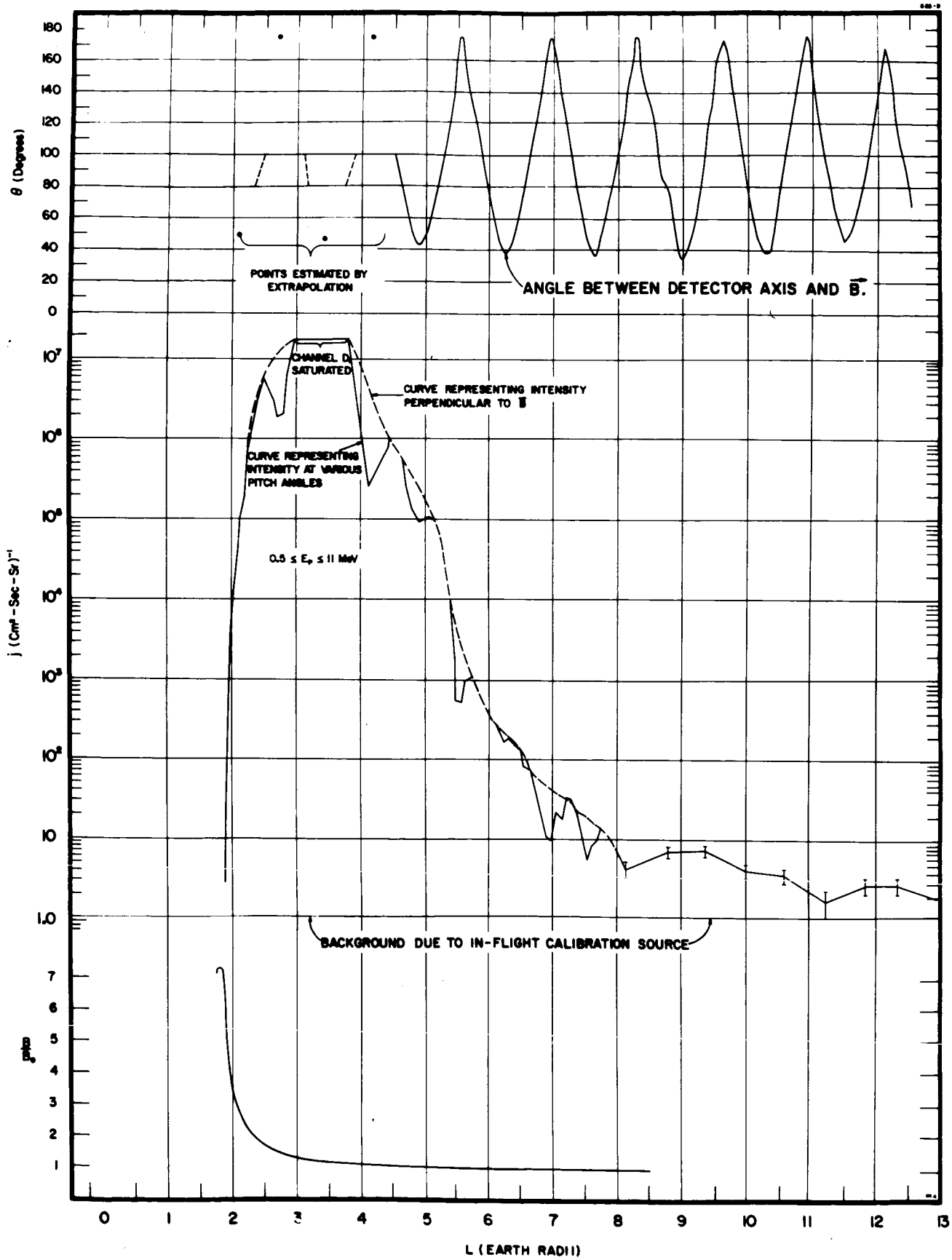
θ (Degrees)
180
160
140
120
100
80
60
40
20
0
POINTS ESTIMATED BY EXTRAPOLATION
ANGLE BETWEEN DETECTOR AXIS AND B.
CHANNEL D SATURATED
CURVE REPRESENTING INTENSITY PERPENDICULAR TO B
CURVE REPRESENTING INTENSITY AT VARIOUS PITCH ANGLES
0.5 ≤ Ep ≤ 11 MeV
j (Cm² - Sec - Sr)⁻¹
10⁷
10⁶
10⁵
10⁴
10³
10²
10
1.0
BACKGROUND DUE TO IN-FLIGHT CALIBRATION SOURCE
counts/sec
7
6
5
4
3
2
1
0
1
2
3
4
5
6
7
8
9
10
11
12
13
L (EARTH RADII)

Figure 6

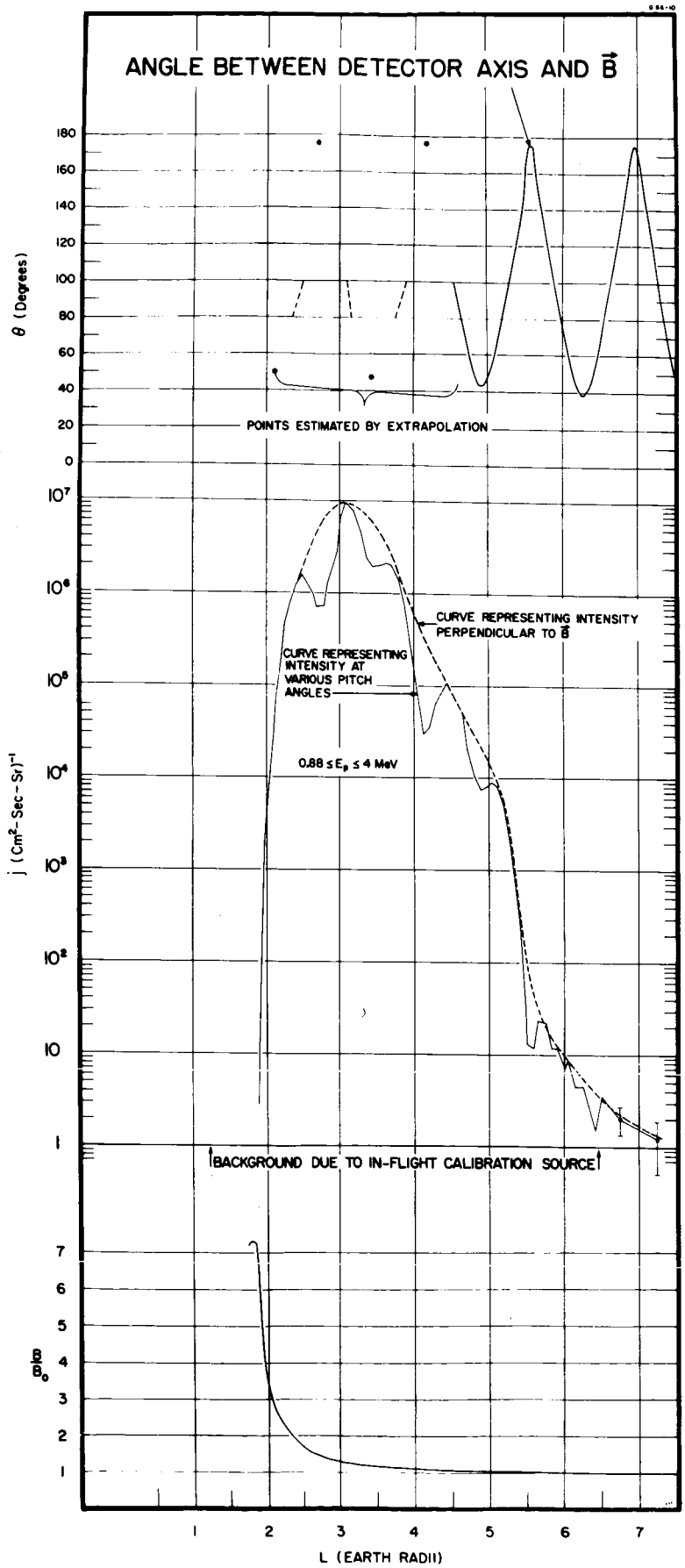
ANGLE BETWEEN DETECTOR AXIS AND $\vec{B}$
θ (Degrees)
180
160
140
120
100
80
60
40
20
0
POINTS ESTIMATED BY EXTRAPOLATION
10^7
10^6
10^5
10^4
10^3
10^2
10
1
j (Cm²-Sec-Sr)⁻¹
CURVE REPRESENTING INTENSITY PERPENDICULAR TO $\vec{B}$
CURVE REPRESENTING INTENSITY AT VARIOUS PITCH ANGLES
$0.88 \leq E_p \leq 4$ MeV
BACKGROUND DUE TO IN-FLIGHT CALIBRATION SOURCE
7
6
5
4
3
2
1
$\frac{B}{B_0}$
1
2
3
4
5
6
7
L (EARTH RADII)

Figure 7

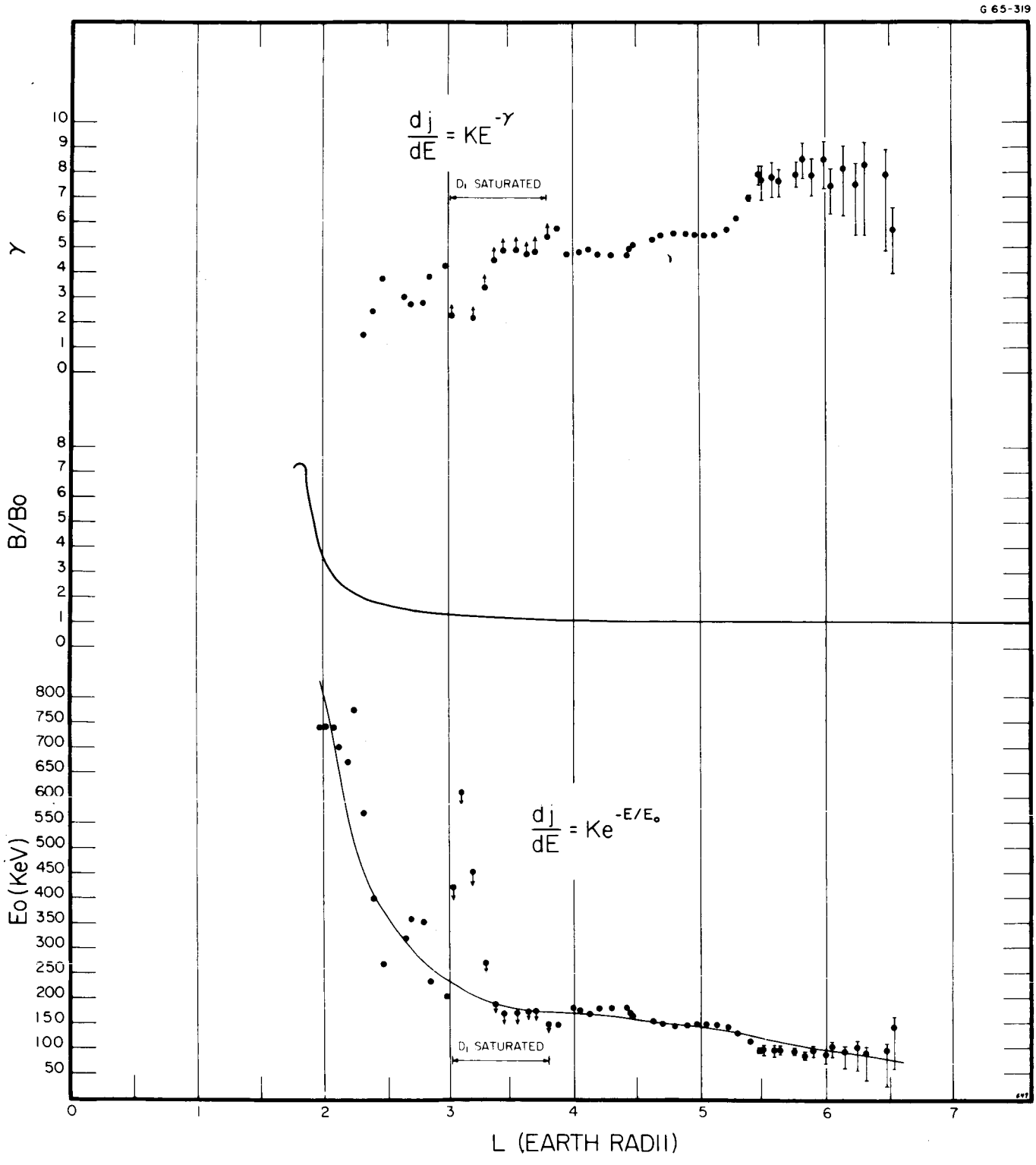
G 65-319
$\frac{dj}{dE} = KE^{-\gamma}$
D_1 SATURATED
γ
B/Bo
Eo (KeV)
$\frac{dj}{dE} = Ke^{-E/E_o}$
D_1 SATURATED
L (EARTH RADII)

Figure 8

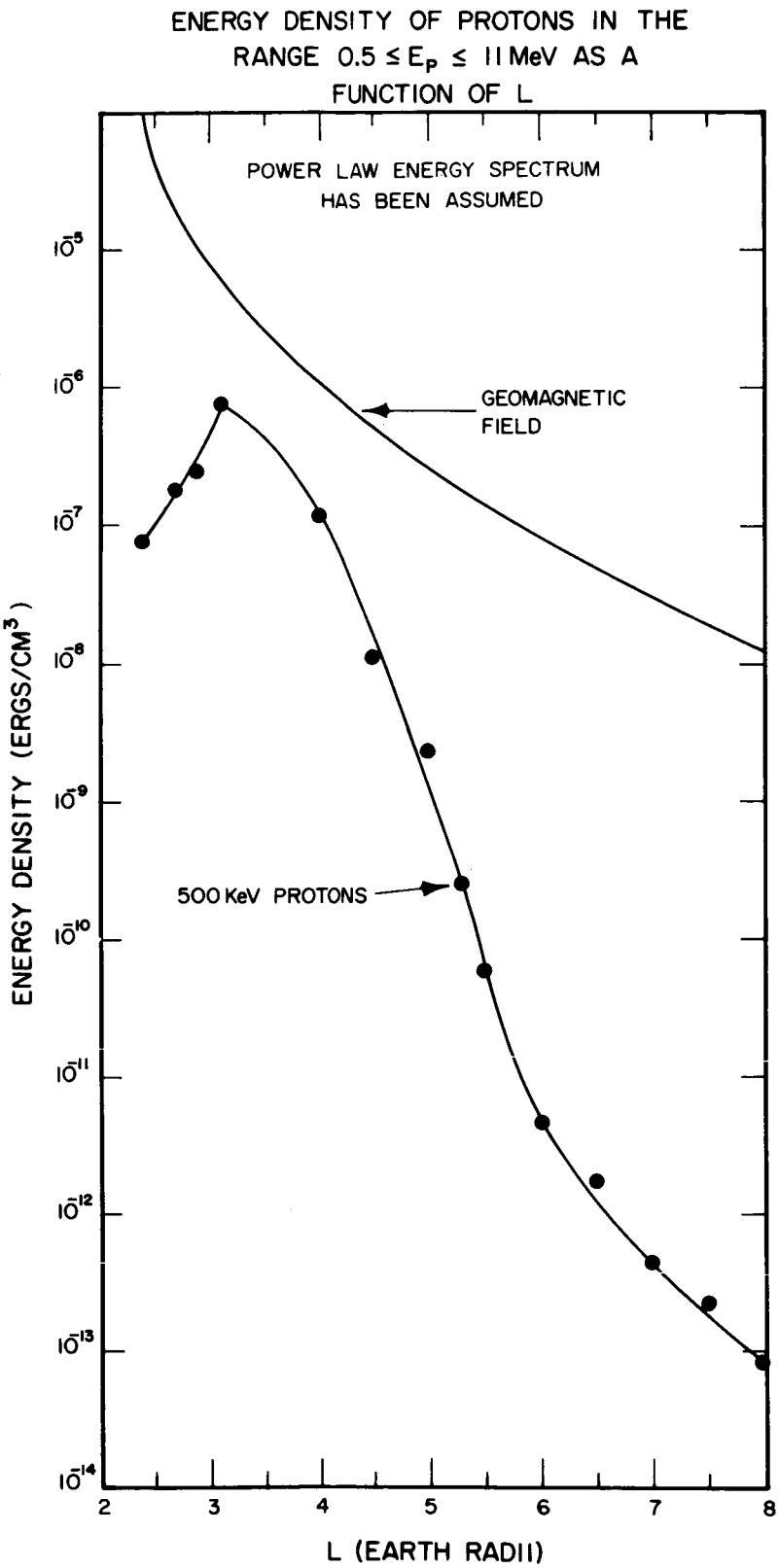
ENERGY DENSITY OF PROTONS IN THE RANGE 0.5 ≤ E_p ≤ 11 MeV AS A FUNCTION OF L
POWER LAW ENERGY SPECTRUM HAS BEEN ASSUMED
GEOMAGNETIC FIELD
500 KeV PROTONS
ENERGY DENSITY (ERGS/CM^3)
10^{-5}
10^{-6}
10^{-7}
10^{-8}
10^{-9}
10^{-10}
10^{-11}
10^{-12}
10^{-13}
10^{-14}
2
3
4
5
6
7
8
L (EARTH RADII)

Figure 9

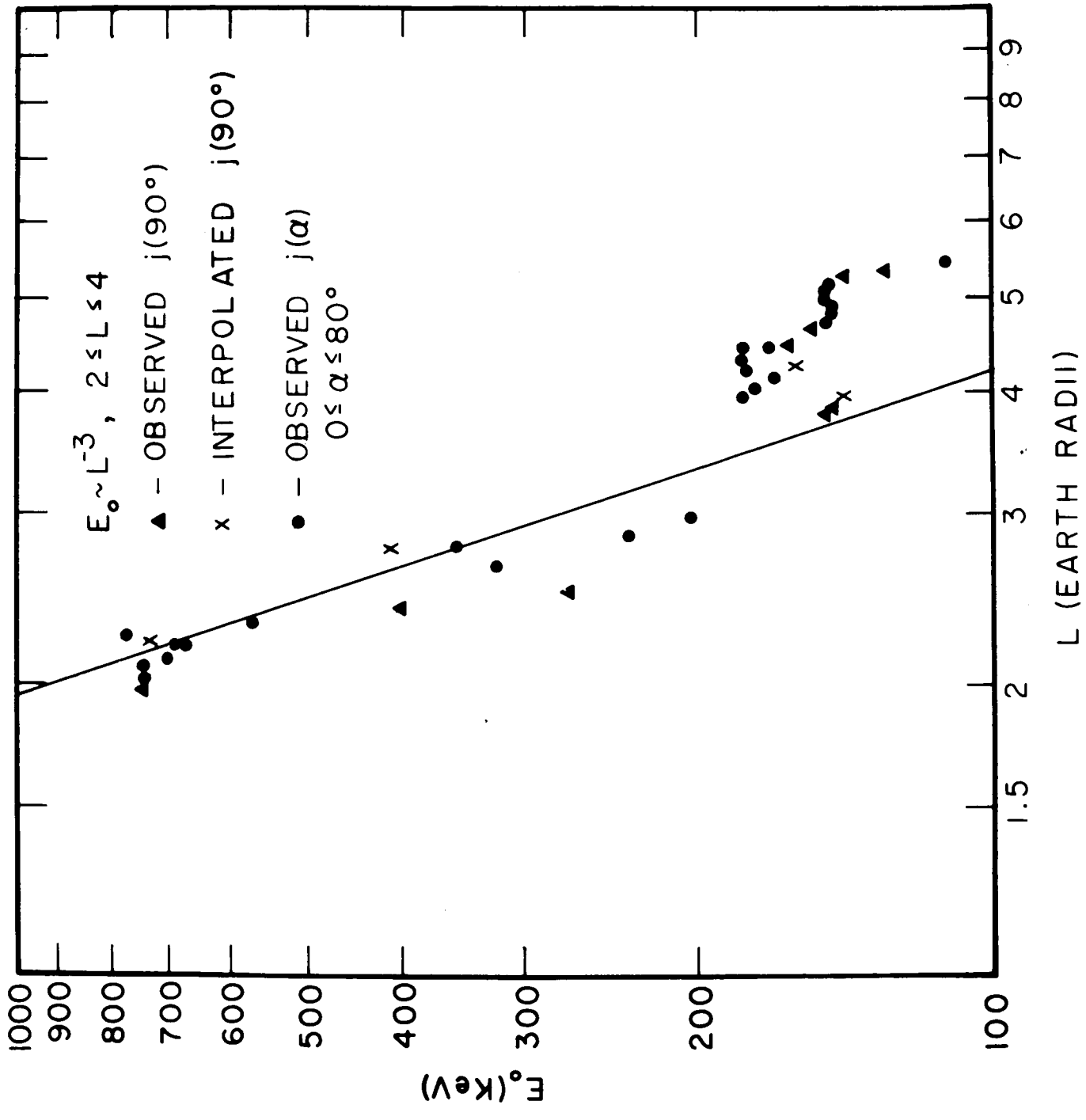
$E_o \sim L^{-3}$, $2 \leq L \leq 4$
▲ – OBSERVED j(90°)
x – INTERPOLATED j(90°)
● – OBSERVED j(α)
$0 \leq \alpha \leq 80°$
E_o(KeV)
1000
900
800
700
600
500
400
300
200
100
1.5
2
3
4
5
6
7
8
9
L (EARTH RADII)

Figure 10